

Supporting Information

Fully conjugated covalent organic frameworks with high conductivity as superior cathode materials for Li-ion batteries

Xudong Qin, Haoran Tang*, Haiyang Zhao, Lin Shao, Chunchen Liu, Lei Ying, and Fei Huang*

X. Qin, Dr. H. Tang, H. Zhao, L. Shao, Dr. C. Liu, Prof. L. Ying, Prof. F. Huang

Institute of Polymer Optoelectronic Materials and Devices

Guangdong Basic Research Center of Excellence for Energy & Information Polymer Materials

State Key Laboratory of Luminescent Materials and Devices

South China University of Technology (SCUT)

Guangzhou, China.

[*] E-mail:

mstanghaoran@scut.edu.cn

msfhuang@scut.edu.cn

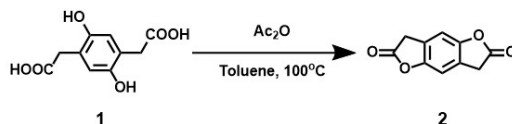
Table of Contents

Section A. Methods and Materials	1
Section B. Supporting Figures	6
Section C. Supporting Tables	15
Section D. Supporting References	19

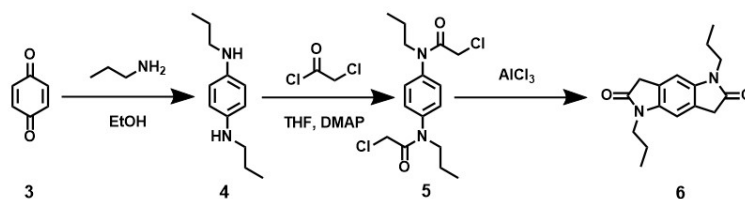
Section A. Methods and Materials.

2,2'-(2,5-dihydroxy-1,4-phenylene) diacetic acid, 1,4-benzophenone, 6-bromoisatin, bromoethyl methyl ether, and 1,3,5-tris(4,4,5,5-tetramethyl-1,3,2-dioxaborolan-2-yl) benzene were purchased from Bide Pharmatech Co. Ltd. n-butanol, acetic acid, and isopropyl alcohol were purchased from J&K Scientific Co. Ltd. Other reagents and chemicals that were not specifically identified were purchased from Energy Chemical.

Fourier transform infrared (FT-IR) spectra were recorded on an IFS 66V/S Fourier transform infrared spectrophotometer. The PXRD data were recorded on a Rigaku model RINT Ultima III diffractometer by depositing powder on a glass substrate, from $2\theta = 2^\circ$ to 25° with 0.01° increment. UV-vis spectra were recorded on a Shimadzu UV-3600 spectrometer. High-resolution transmission electron microscopy (HR-TEM) images were obtained on a TEM JEOL 2100F with an acceleration voltage of 300 kV. X-ray photoelectron spectroscopy (XPS) analysis was conducted using the Thermo Scientific K-Alpha. Gas sorption isotherms were measured on a BELSORP-mini (MicrotracBEL, Japan, Corp.) automated volumetric sorption analyzer. The desired temperature (77 K) was controlled by a liquid nitrogen bath. The conductivity measurements were conducted on JouleYacht MRS-3RT. The conductivity σ was calculated based on the equation $\sigma = IL/VWd$, where I represents the current, V represents the voltage, L represents the voltage probe distance (3.6 mm), W represents the sample width (10 mm) and d represents the thickness of the sample.



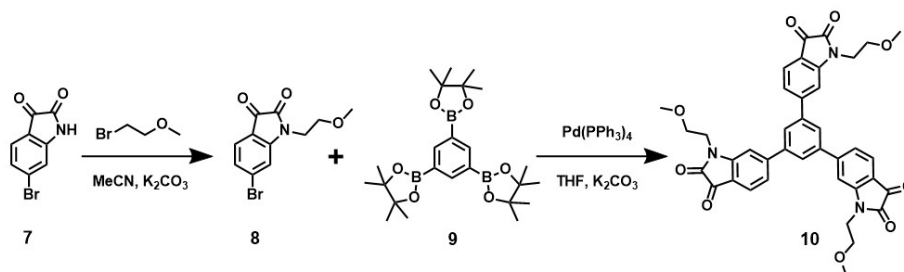
Synthesis of 3,7-dihydrobenzo[1,2-b:4,5-b'] difuran-2,6-dione (2, H-BFDO). H-BFDO was synthesized following previously reported procedures.^{1,2} To a suspension of compound **1** (1.0 g, 4.4 mmol) in anhydrous toluene (50 mL), Ac₂O (10 mL) was added. The mixture was stirred at 100°C for 5 h and then the solvent was removed under reduced pressure. The residue was purified by recrystallization from toluene to give **2** as a white powder (0.79 g, 80 %). ¹H NMR (CDCl₃, 400 MHz, ppm): δ 7.07 (s, 2H), 3.78 (s, 4H).



Synthesis of N¹, N⁴-dipropylbenzene-1,4-diamine (4). Compound **3** (21.49 g, 191.6 mmol), n-propylamine (23.26 g, 393.5 mmol) were added to ethanol (600 mL) and reacted in air for 1 h. Evaporation of the solvent yielded the crude product, which was used directly without purification.

Synthesis of N, N'-(1,4-phenylene) bis(2-chloro-N-propylacetamide) (5). Compound **4** (9.0 g, 46.8 mmol), 4-dimethylaminopyridine (5.72 g, 46.82 mmol) were added to tetrahydrofuran (THF, 200 mL) in a 1000 mL round bottom flask. Then, chloroacetic chloride (15.9 g, 140.78 mmol) dissolved in 250 mL THF was added dropwise to the reaction system. The mixture was stirred for 1h at room temperature under nitrogen atmosphere. The solvent was removed under vacuum using rotary evaporation. The product was purified by silica gel column chromatography using petroleum ether/dichloromethane (PE/DCM, v/v = 1/1) as the eluent.

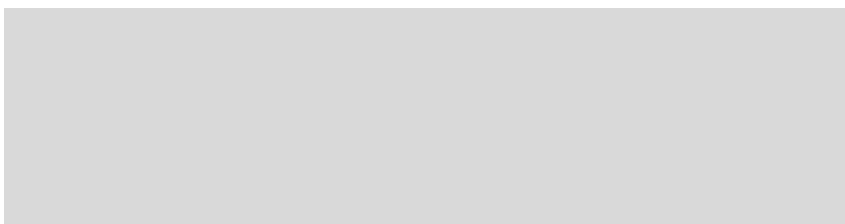
Synthesis of 1,5-dipropyl-5,7-dihydropyrrolo[2,3-f] indole-2,6(1H,3H)-dione (6, H-BPDO). Compound **5** (1 g, 2.84 mmol), and AlCl₃ (2.7 g, 20.25 mmol) was added into a 50 mL single-necked reaction flask and reacted at 190°C for 40 min under nitrogen atmosphere. The reaction was then cooled to room temperature and quenched with water. The solids were filtered out as crude product, which was subsequently purified by silica gel column chromatography using DCM/PE (v/v = 10/1) to obtain a white product. Yield 500 mg (64%). ¹H NMR (CDCl₃, 400 MHz, ppm): 6.79 (s, 2H), 3.68-3.65 (m, 4H), 3.55 (s, 4H), 1.72-1.68 (m, 4H), 0.99-0.96 (m, 6H).



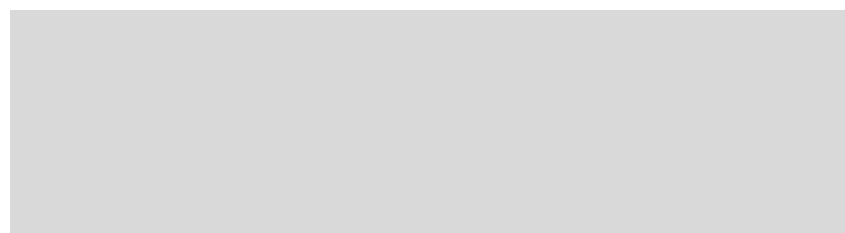
Synthesis of 6-bromo-1-(2-methoxyethyl)-1H-indole-2,3-dione (8). The 6-bromo-1-(2-methoxyethyl)-1H-indole-2,3-dione was synthesized by adding 6-bromoisatin (5 g, 22.33 mmol), K₂CO₃ (4.62 g, 33.5 mmol), and MeCN (200 mL) to a 500 ml double-necked reaction flask. The mixture was heated at 80°C for half an hour, and then bromoethyl methyl ether (4.62g, 33.5 mmol) was added. After being heated for 12 hours, the reaction was cooled to room temperature and quenched with water, followed by extraction with ethyl acetate, collection of the organic phase, and drying by addition

of MgSO₄. Finally, purification of the product was carried out by chromatography over the column PE/DCM (v/v = 1/1) to obtain an orange product.

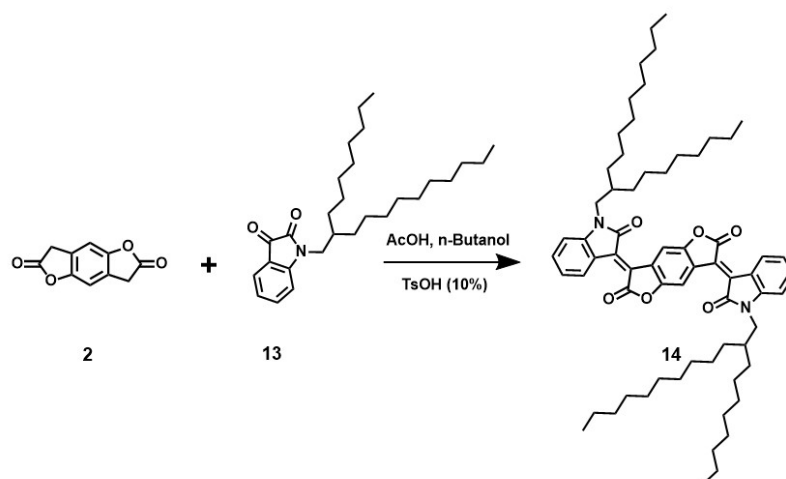
Synthesis of 6,6',6''-(benzene-1,3,5-triyl)tris(1-(2-methoxyethyl)indoline-2,3-dione) (10, TBI). A reaction mixture containing compound **9** (2.02 g, 8.00 mmol), Pd(PPh₃)₄ (506 mg, 0.40 mmol), compound **8** (5.16 g, 18.24 mmol), and K₂CO₃ (5.52 g, 40 mmol) in THF (100 mL) and H₂O (20 mL) was stirred under argon at 80°C for 3 days. After cooling to room temperature, the yellow precipitate was collected by filtration, washed with cyclohexane and acetone to yield the product as a bright yellow powder. Yield: 2.6 g (86%). ¹H NMR (CDCl₃, 400 MHz, ppm): δ 7.86 (s, 3H), 7.74-7.73 (d, 3H), 7.42-7.40 (d, 3H), 7.34 (s, 3H), 4.01-3.99 (m, 6H), 3.72-3.69 (m, 6H), 3.35 (s, 9H).



Synthesis of 3,7-bis((E)-6-bromo-1-(2-methoxyethyl)-2-oxoindolin-3-ylidene)-3,7-dihydrobenzo[1,2-b:4,5-b']difuran-2,6-dione (11). The H-BFDO (190.1 mg, 1.0 mmol), and compound **8** (594.3 mg, 2.1 mmol) were added in a 25ml double necked bottle with 5 mL of AcOH/n-Butanol (v/v = 1/1) as solution. Subsequently, p-toluenesulfonic acid (0.1 eq) was added as a catalyst. The mixture was subjected to a vacuum reaction at 130°C for 24 hours. The reaction was restored to room temperature. The precipitate was filtered and washed with methanol to give crude product. HR-MS (MALDI) m/z calcd. for (C₃₂H₂₁Br₂N₂O₈) (M-H⁺): 720.97. Found: 720.66.

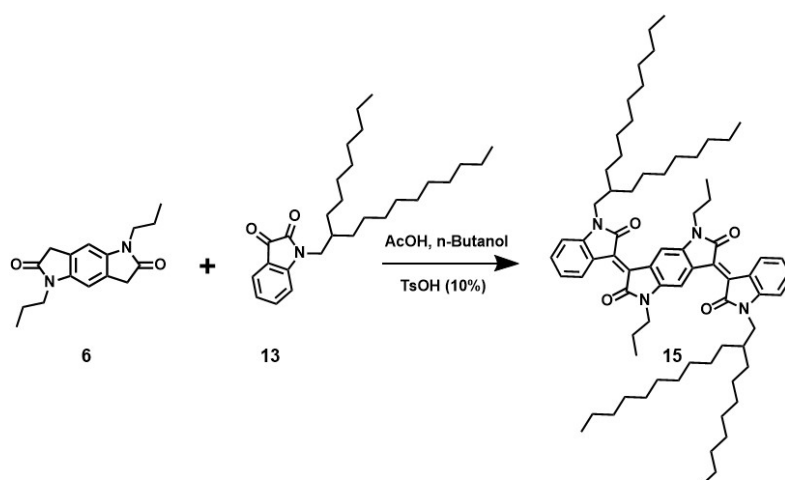


Synthesis of 3,7-bis((E)-6-bromo-1-(2-methoxyethyl)-2-oxoindolin-3-ylidene)-1,5-dipropyl-5,7-dihydropyrrolo[2,3-f]indole-2,6(1H,3H)-dione (12). The H-BPDO (272.2 mg, 1 mmol), and compound **8** (594.3 mg, 2.1 mmol) were added in a 25ml double necked bottle with 5 mL of AcOH/n-Butanol (v/v = 1/1) reaction solution. Subsequently, p-toluenesulfonic acid (0.1 eq) was added as a catalyst. The mixture was subjected to a vacuum reaction at 130°C for 24 hours. The reaction was restored to room temperature. The precipitate was filtered and washed with methanol to give crude product. HR-MS (MALDI) m/z calcd. for (C₃₈H₃₅Br₂N₄O₂) (M-H⁺): 803.10. Found: 802.64.



Synthesis of 3,7-bis((E)-1-(2-hexyldecyl)-2-oxoindolin-3-ylidene)-3,7-dihydrobenzo[1,2-b:4,5-b']difuran-2,6-dione (14).

The H-BFDO (190.1 mg, 1.0 mmol), and compound **13** (868.7 mg, 2.1 mmol) were added in a 25 mL double-necked bottle with 5 mL of AcOH/n-Butanol (v/v = 1/1) as solution. Subsequently, p-toluenesulfonic acid (0.1 eq) was added as a catalyst. The mixture was subjected to a vacuum reaction at 130°C for 24 hours. The reaction was restored to room temperature. The precipitate was filtered and washed with methanol. Yield 844.0 mg (86%). ¹H NMR (CDCl₃, 400 MHz, ppm): δ 9.13 (s, 2H), 9.06-9.04 (m, 2H), 7.42-7.39 (m, 2H), 7.09-7.06 (m, 2H), 6.80-6.78 (d, 2H), 3.67-3.66 (d, 4H), 1.92-1.89 (m, 2H), 1.34-1.23 (m, 64H), 0.87-0.84 (m, 12H).



Synthesis of 3,7-bis((E)-1-(2-hexyldecyl)-2-oxoindolin-3-ylidene)-1,5-dipropyl-5,7-dihydropyrrolo[2,3-f]indole-

2,6(1H,3H)-dione (15). The H-BPDO (272.2 mg, 1.0 mmol), and compound **13** (868.7 mg, 2.1 mmol) were added in a 25 mL double-necked bottle with 5 mL of AcOH/n-Butanol (v/v = 1/1) as solution. Subsequently, p-toluenesulfonic acid (0.1 eq) was added as a catalyst. The mixture was subjected to a vacuum reaction at 130°C for 24 hours. The reaction was restored to room temperature. The precipitate was filtered and washed with methanol. Yield 893.4 mg (84%). ¹H NMR (CDCl₃, 400 MHz, ppm): δ 9.23-9.21 (m, 2H), 8.87 (s, 2H), 7.36-7.33 (m, 2H), 7.06-7.02 (m, 2H), 6.77-6.75 (d, 2H), 3.85-3.83 (m, 4H), 3.68-3.66 (d, 4H), 1.89-1.81 (m, 6H), 1.27-1.23 (m, 64H), 0.87-0.86 (m, 6H), 0.85-0.84 (m, 12H).

Synthesis of TBI-COF-O. H-BFDO (5.7 mg, 0.03 mmol) and TBI (13.8 mg, 0.02 mmol) were added into AcOH/n-Butanol (1 mL, v/v = 1/1) solution in a 10 mL Pyrex tube. Then 4M TsOH in isopropanol was added to the solution as a catalyst. The tube was degassed by three freeze-pump-thaw cycles. After that, the tube was sealed off and heated to 120°C for 4 days. The precipitates were collected by centrifugation and then washed with THF (3 × 10 mL), acetone (3 × 10 mL), DCM (3 × 10 mL), and the powder was placed in a Soxhlet extractor and washed with chlorobenzene. Finally, the powder was collected and dried at 80°C under vacuum overnight to give **TBI-COF-O** in a yield of 87%.

Synthesis of TBI-COF-N. H-BPDO (8.2 mg, 0.03 mmol) and TBI (13.8 mg, 0.02 mmol) were added into AcOH/n-Butanol (1 mL, v/v = 1/1) solution in a 10 mL Pyrex tube. Then 4M TsOH in isopropanol was added to the solution as a base catalyst. The tube was degassed by three freeze-pump-thaw cycles. After that, the tube was sealed off and heated to 140°C for 4 days. The precipitates were collected by centrifugation and then washed with tetrahydrofuran (3 × 10 mL), acetone (3 × 10 mL), DCM (3 × 10 mL), and the powder was placed in a Soxhlet extractor and washed with chlorobenzene. Finally, the powder was collected and dried at 80 °C under vacuum overnight to give **TBI-COF-N** in a yield of 82%.

Computational Calculation. The PXRD data were analyzed by Pawley refinement using Reflex, which is a commercial software package for crystallographic structural analysis implemented in MS modeling version 4.4 (Accelrys Inc.). The final R_{WP} and R_p values were calculated as 3.74% and 6.26% for **TBI-COF-O**. Meanwhile, the final R_{WP} and R_p values were calculated as 6.89% and 11.24% for **TBI-COF-N**. Unit cell dimensions were solved manually using coordinates from the obtained PXRD pattern positions. Pawley refinement was then performed, and the lattice parameters were iteratively optimized until the R_{WP} values converged.

Computational details. The geometry of an isolated molecule and complexes was optimized at the B3LYP-D3(BJ)/6-311+G(d, p) level using the Gaussian 09 software package.

Electrochemical Measurements. The electrodes were prepared by casting a mixture of **TBI-COF-O** (or **TBI-COF-N**), carbon black and polyvinylidene difluoride (PVDF) with a mass ratio of 7:2:1/8:1:1 onto a copper foil. Polyethylene membrane was used as the separator. The electrolyte was 1 M LiPF₆ in ethylene carbonate: dimethyl carbonate (EC/DMC, v/v = 1/1). The electrochemical performances were tested in 2032-coin cells with a 450 μm Li as the cathode. The LAND battery test system (CT2001A) was used for long-term cyclic stability and rate capability tests. An electrochemical work station (CHI760D) was used to obtain the data of cyclic voltammetry (CV) and electrochemical impedance spectroscopy (EIS). The EIS was tested within a frequency range of 0.01-100000 Hz and a voltage amplitude of 5 mV.

Theoretical capacity calculations. The theoretical capacities (C_t , mAh g⁻¹) of **TBI-COF-O** and **TBI-COF-N** were calculated according to the following equation (2):

$$C_t = \frac{nF}{3.6M}$$

Where n is the number of transferred electrons during the redox reaction, and M is the molecular weight of the unit cell of **TBI-COF-O** and **TBI-COF-N**, F is the Faraday constant (96500 C mol⁻¹).

Pseudo capacitance calculations. To evaluate the capacitive contribution of **TBI-COF-O**, and **TBI-COF-N** to the total current response, the diffusion-controlled and surface capacitive contributions can quantitatively be separated using the equation (3) below:

$$i = kV + bV^{\frac{1}{2}}$$

where v is the scan rate, i is the current, k and b are constants.

Section B. Supporting Figures

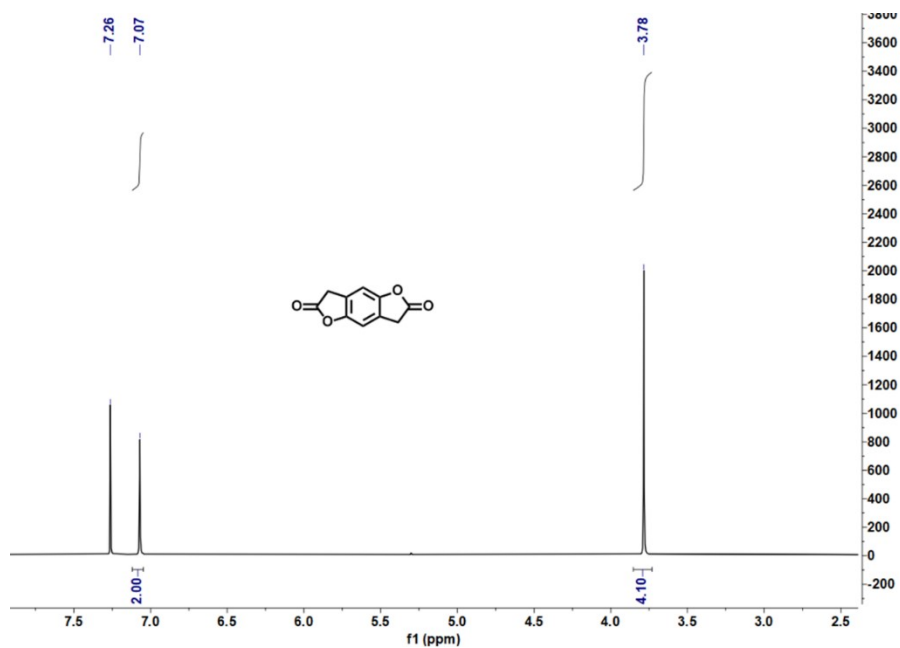


Figure S1. ¹H NMR spectrum of H-BFDO.

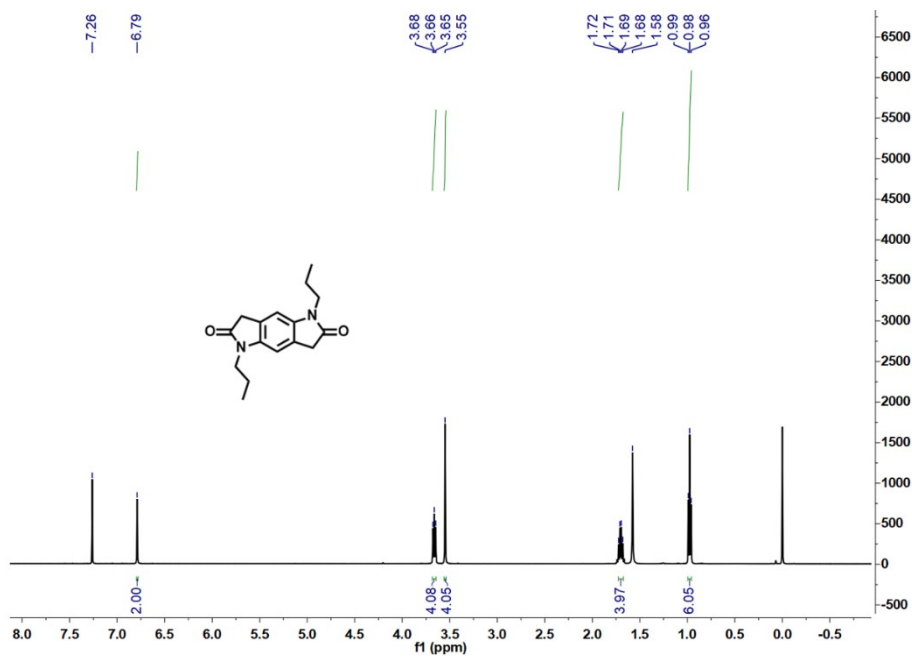


Figure S2. ¹H NMR spectrum of H-BPDO.

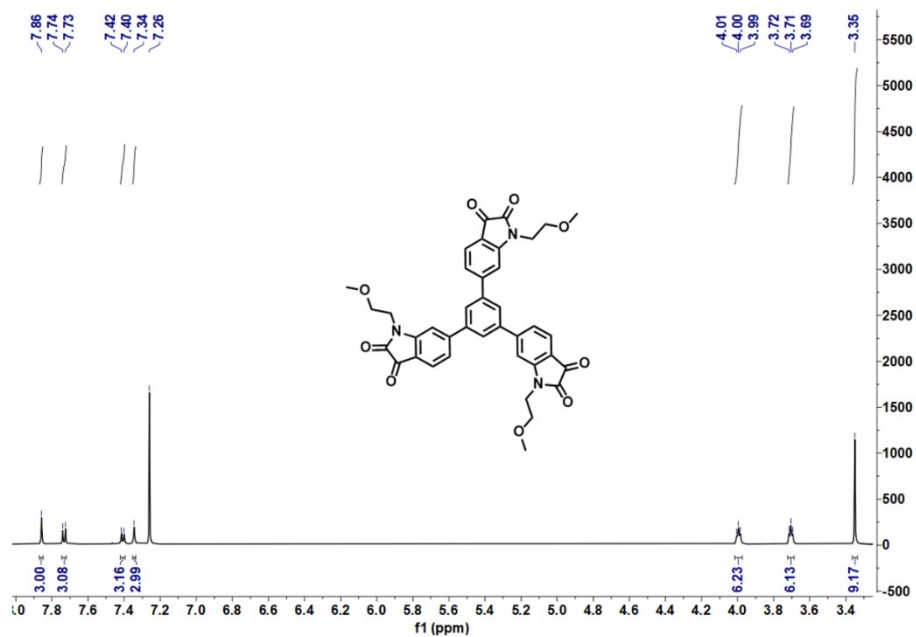


Figure S3. ^1H NMR spectrum of TBI.

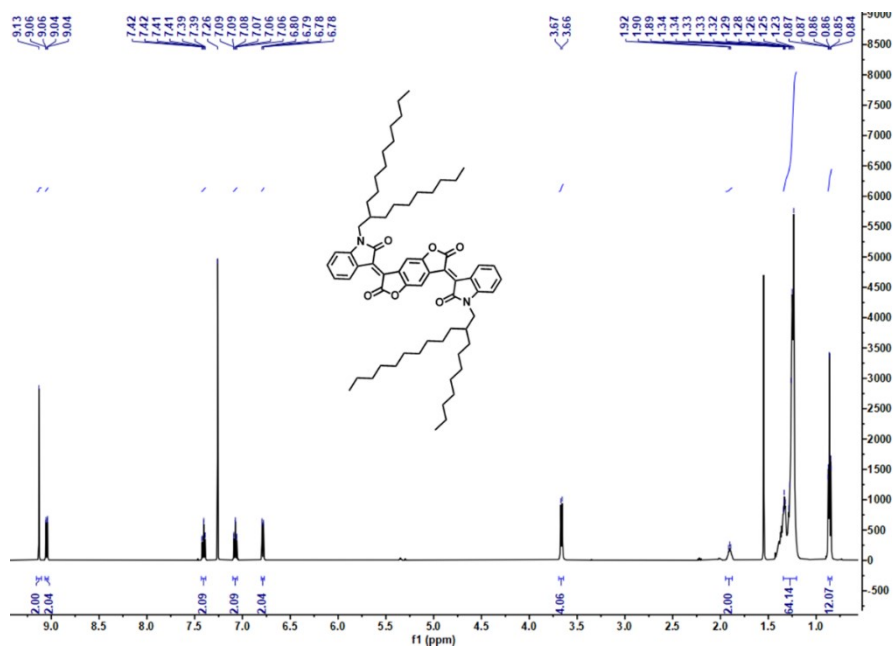


Figure S4. ^1H NMR spectrum of compound 14.

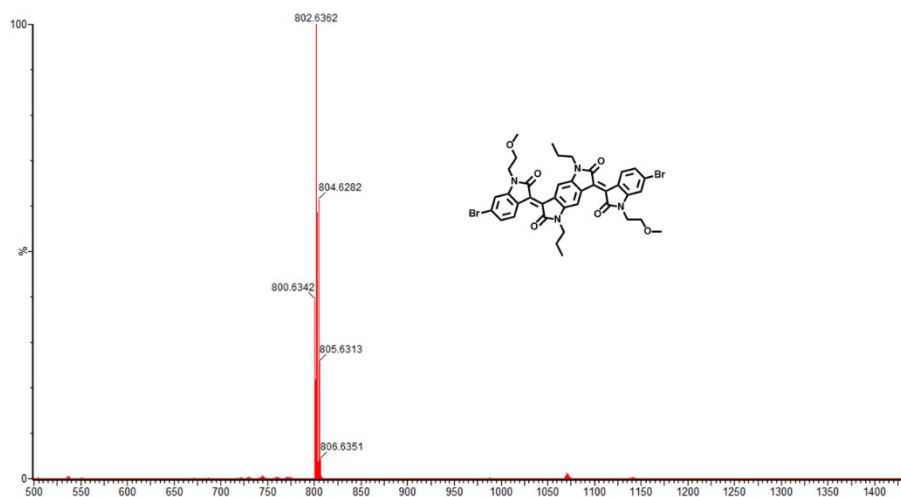


Figure S7. Mass spectrum of compound 12.

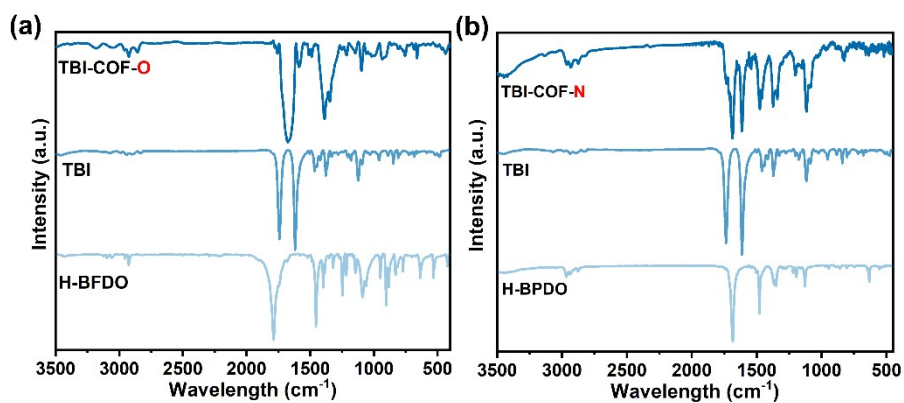


Figure S8. The FT-IR spectra of (a) TBI-COF-O, and (b) TBI-COF-N.

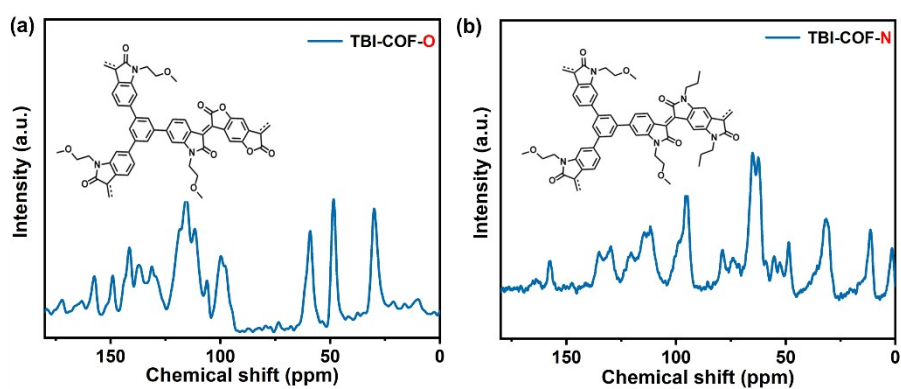


Figure S9. The solid-state ^{13}C NMR of (a) TBI-COF-O, and (b) TBI-COF-N.

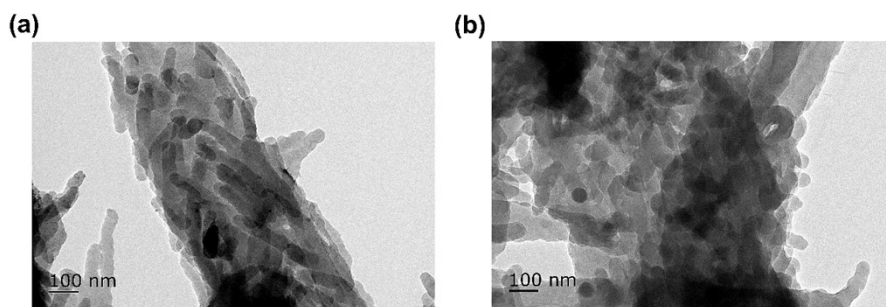


Figure S10. HR-TEM of (a) TBI-COF-O, and (b) TBI-COF-N.

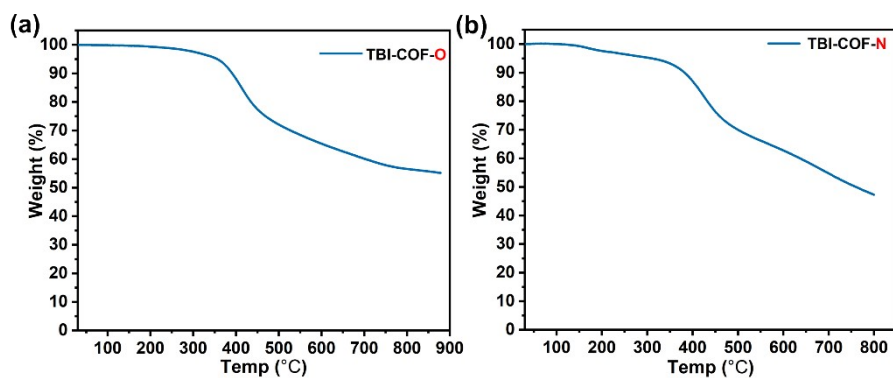


Figure S11. The thermogravimetric investigations of (a) TBI-COF-O, and (b) TBI-COF-N.

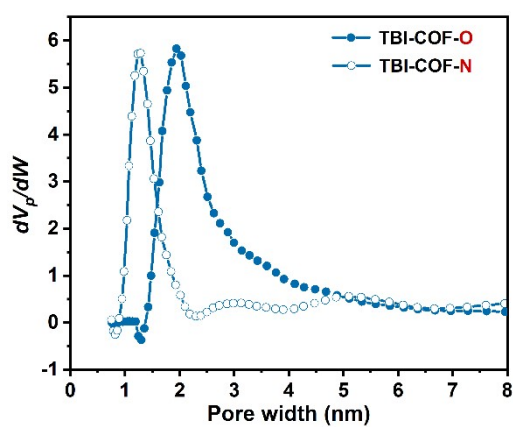


Figure S12. Pore size distribution profile of TBI-COF-O and TBI-COF-N.

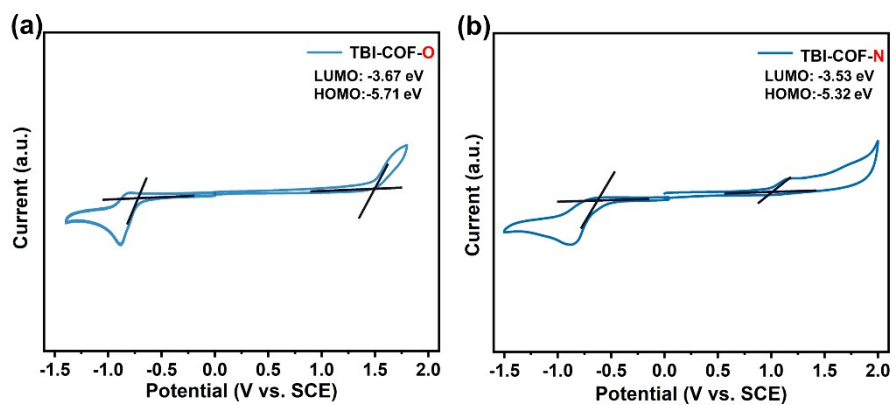


Figure S13. The electrochemical energy level of (a) TBI-COF-O, and (b) TBI-COF-N.

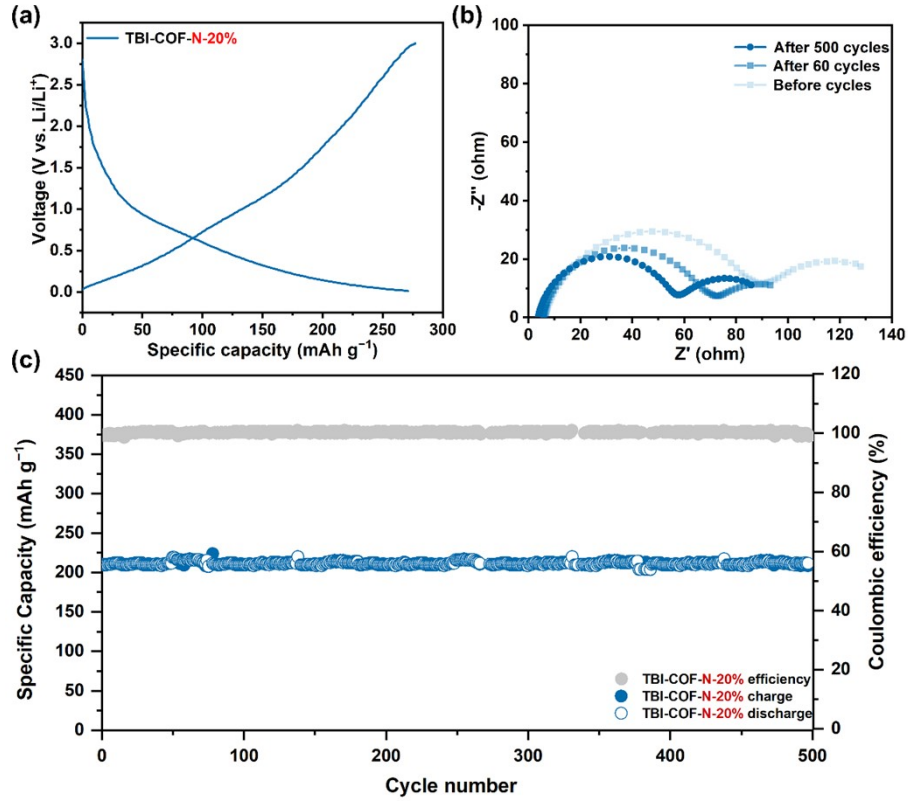


Figure S14. Lithium-ion battery performance with COF-based cathodes. (a) Specific capacity of TBI-COF-N with 20wt% conductive carbon at the rate of 0.1C; (b) Electrochemical impedance spectra of TBI-COF-N under different cycles. (c) Long-term cycling stability of TBI-COF-N cathodes at a discharge rate of 1C.

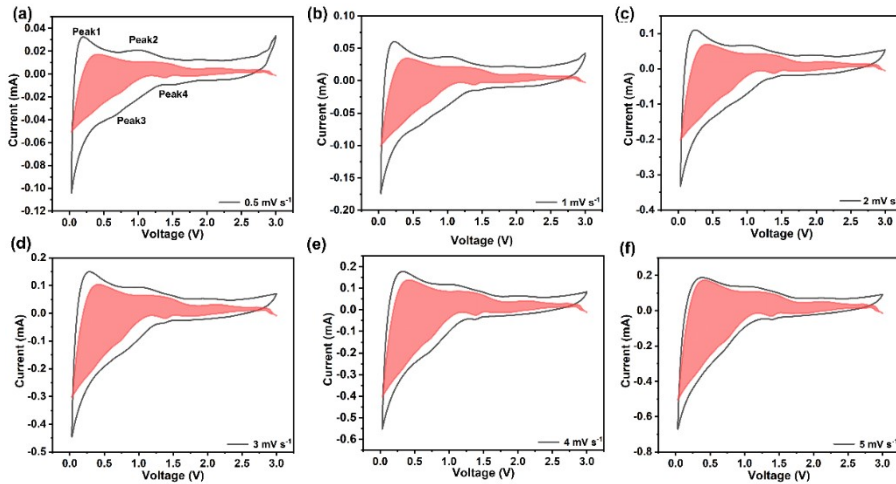


Figure S15. The cyclic voltammetry (CV) curves and the integral area of the origin region (red area) of TBI-COF-O under different scan rates, (a) 0.5 mV s⁻¹, (b) 1 mV s⁻¹, (c) 2 mV s⁻¹, (d) 3 mV s⁻¹, (e) 4 mV s⁻¹, and (f) 5 mV s⁻¹.

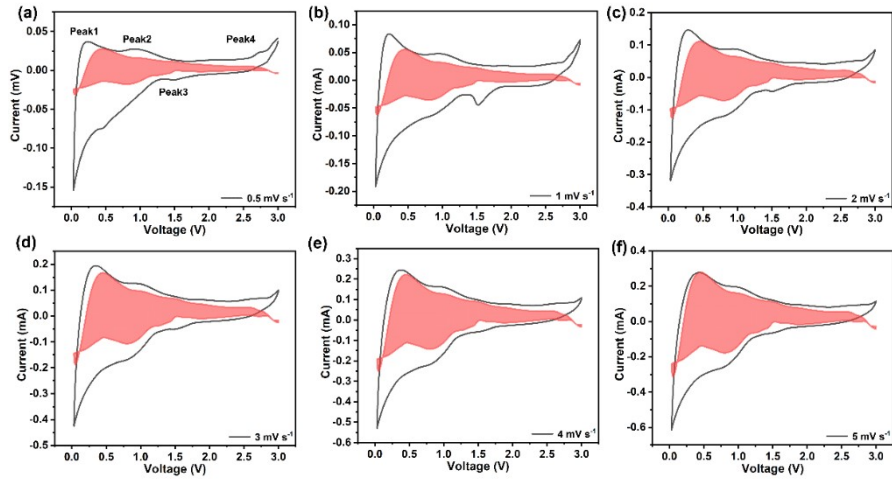


Figure S16. The cyclic voltammetry (CV) curves and the integral area of the origin region (red area) of **TBI-COF-N** under different scan rates, (a) 0.5 mV s^{-1} , (b) 1 mV s^{-1} , (c) 2 mV s^{-1} , (d) 3 mV s^{-1} , (e) 4 mV s^{-1} , and (f) 5 mV s^{-1} .

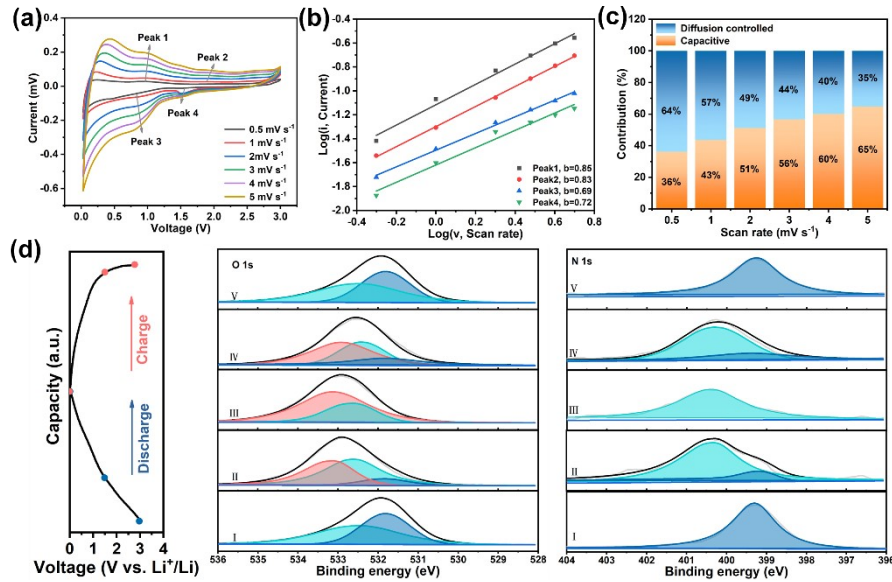


Figure S17. (a) The cyclic voltammetry (CV) curves of **TBI-COF-N** under different scan rates (0.5 mV s^{-1} , 1 mV s^{-1} , 2 mV s^{-1} , 3 mV s^{-1} , 4 mV s^{-1} , and 5 mV s^{-1}); (b) Linear fits of the logarithms of the peak current against logarithms of scan rate for **TBI-COF-N**; (c) Normalized capacity contribution of the capacitive and diffusion-controlled process of the **TBI-COF-N**; (d) Ex-situ X-ray photoelectron spectroscopy energy spectra of **TBI-COF-N** corresponding to the charging and discharging behaviors of the battery, including O1s, and N1s.

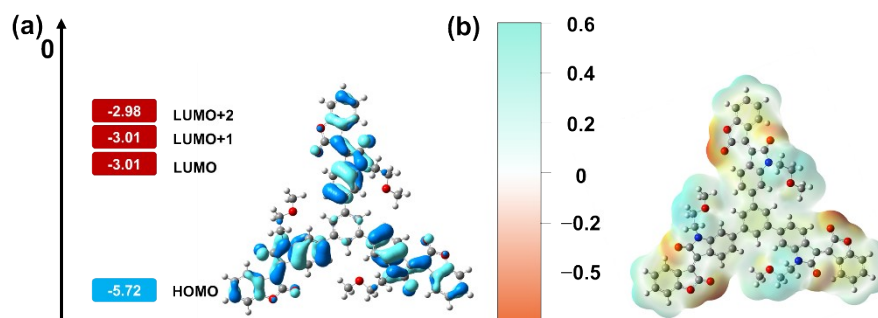


Figure S18. (a) Theoretical calculation results of **TBI-COF-O**; (b) Electrostatic potential map of **TBI-COF-O** (red color represents the preferred binding site for Li^+).

Section C. Supporting Tables

Table S1. Optimization of synthesis conditions for **TBI-COF-O**.

Entry No.	Solvents	Catalyst	Temperature (°C)	Crystallinity
1	o-DCB/n-BuOH=1/1	2M Na ₂ CO ₃	120	No
2	o-DCB/n-BuOH=1/1	2M NaOH	120	No
3	o-DCB/n-BuOH=1/1	2M KOH	120	No
4	o-DCB/n-BuOH=1/1	Pyridine	120	No
5	o-DCB/n-BuOH=1/1	Piperidine	120	No
6	o-DCB/n-BuOH=1/1	Et ₃ N	120	No
7	o-DCB/n-BuOH=1/1	AcOH	120	No
8	o-DCB/n-BuOH=1/1	6M AcOH	120	No
9	o-DCB/n-BuOH=1/1	12M AcOH	120	No
10	o-DCB/n-BuOH=1/1	CF ₃ SO ₃ H	120	No
11	o-DCB/n-BuOH=1/1	TsOH	120	No
12	o-DCB/n-BuOH=1/1	2M TsOH	120	No
13	o-DCB/n-BuOH=1/1	4M TsOH	120	No
14	o-DCB/n-BuOH=1/1	6M TSOH	120	No
15	Dioxane/Mes=1/1	2M Na ₂ CO ₃	120	No
16	Dioxane/Mes=1/1	2M NaOH	120	No
17	Dioxane/Mes=1/1	2M KOH	120	No
18	Dioxane/Mes=1/1	Pyridine	120	No
19	Dioxane/Mes=1/1	Piperidine	120	No
20	Dioxane/Mes=1/1	Et ₃ N	120	No
21	Dioxane/Mes=1/1	AcOH	120	No
22	Dioxane/Mes=1/1	6M AcOH	120	No
23	Dioxane/Mes=1/1	12M AcOH	120	No
24	Dioxane/Mes=1/1	CF ₃ SO ₃ H	120	No
25	Dioxane/Mes=1/1	TsOH	120	No
26	Dioxane/Mes=1/1	2M TsOH	120	No
27	Dioxane/Mes=1/1	4M TsOH	120	No
28	Dioxane/Mes=1/1	6M TSOH	120	No
29	DMF/n-BuOH=1/1	2M Na ₂ CO ₃	120	No
30	DMF/n-BuOH=1/1	2M NaOH	120	No
31	DMF/n-BuOH=1/1	2M KOH	120	No
32	DMF/n-BuOH=1/1	Pyridine	120	No
33	DMF/n-BuOH=1/1	Piperidine	120	No
34	DMF/n-BuOH=1/1	Et ₃ N	120	No
35	DMF/n-BuOH=1/1	AcOH	120	No
36	DMF/n-BuOH=1/1	6M AcOH	120	No
37	DMF/n-BuOH=1/1	12M AcOH	120	No
38	DMF/n-BuOH=1/1	CF ₃ SO ₃ H	120	No
39	DMF/n-BuOH=1/1	TsOH	120	No
40	DMF/n-BuOH=1/1	2M TsOH	120	No
41	DMF/n-BuOH=1/1	4M TsOH	120	No
42	DMF/n-BuOH=1/1	6M TSOH	120	No
43	DMAc/n-BuOH =1/1	2M Na ₂ CO ₃	120	No
44	DMAc/n-BuOH =1/1	2M NaOH	120	No
45	DMAc/n-BuOH =1/1	2M KOH	120	No
46	DMAc/n-BuOH =1/1	Pyridine	120	No
47	DMAc/n-BuOH =1/1	Piperidine	120	No
48	DMAc/n-BuOH =1/1	Et ₃ N	120	No
49	DMAc/n-BuOH =1/1	AcOH	120	No

50	DMAC/n-BuOH =1/1	6M AcOH	120	No
51	DMAC/n-BuOH =1/1	12M AcOH	120	No
52	DMAC/n-BuOH =1/1	CF ₃ SO ₃ H	120	No
53	DMAC/n-BuOH =1/1	TsOH	120	No
54	DMAC/n-BuOH =1/1	2M TsOH	120	No
55	DMAC/n-BuOH =1/1	4M TsOH	120	No
56	DMAC/n-BuOH =1/1	6M TSOH	120	No
57	AcOH	4M TsOH	120	Low
58	AcOH/n-BuOH=1/1	4M TsOH	120	High
59	AcOH/isopropanol=1/1	4M TsOH	120	High

Table S2. Optimization of synthesis conditions for **TBI-COF-N**.

Entry No.	Solvents	Catalyst	Temperature (°C)	Crystallinity
1	o-DCB/n-BuOH=1/1	2M Na ₂ CO ₃	120	No
2	o-DCB/n-BuOH=1/1	2M NaOH	120	No
3	o-DCB/n-BuOH=1/1	2M KOH	120	No
4	o-DCB/n-BuOH=1/1	Pyridine	120	No
5	o-DCB/n-BuOH=1/1	Piperidine	120	No
6	o-DCB/n-BuOH=1/1	Et ₃ N	120	No
7	o-DCB/n-BuOH=1/1	AcOH	120	No
8	o-DCB/n-BuOH=1/1	6M AcOH	120	No
9	o-DCB/n-BuOH=1/1	12M AcOH	120	No
10	o-DCB/n-BuOH=1/1	CF ₃ SO ₃ H	120	No
11	o-DCB/n-BuOH=1/1	TsOH	120	No
12	o-DCB/n-BuOH=1/1	2M TsOH	120	No
13	o-DCB/n-BuOH=1/1	4M TsOH	120	No
14	o-DCB/n-BuOH=1/1	6M TSOH	120	No
15	Dioxane/Mes=1/1	2M Na ₂ CO ₃	120	No
16	Dioxane/Mes=1/1	2M NaOH	120	No
17	Dioxane/Mes=1/1	2M KOH	120	No
18	Dioxane/Mes=1/1	Pyridine	120	No
19	Dioxane/Mes=1/1	Piperidine	120	No
20	Dioxane/Mes=1/1	Et ₃ N	120	No
21	Dioxane/Mes=1/1	AcOH	120	No
22	Dioxane/Mes=1/1	6M AcOH	120	No
23	Dioxane/Mes=1/1	12M AcOH	120	No
24	Dioxane/Mes=1/1	CF ₃ SO ₃ H	120	No
25	Dioxane/Mes=1/1	TsOH	120	No
26	Dioxane/Mes=1/1	2M TsOH	120	No
27	Dioxane/Mes=1/1	4M TsOH	120	No
28	Dioxane/Mes=1/1	6M TSOH	120	No
29	DMF/n-BuOH=1/1	2M Na ₂ CO ₃	120	No
30	DMF/n-BuOH=1/1	2M NaOH	120	No
31	DMF/n-BuOH=1/1	2M KOH	120	No
32	DMF/n-BuOH=1/1	Pyridine	120	No
33	DMF/n-BuOH=1/1	Piperidine	120	No
34	DMF/n-BuOH=1/1	Et ₃ N	120	No
35	DMF/n-BuOH=1/1	AcOH	120	No
36	DMF/n-BuOH=1/1	6M AcOH	120	No
37	DMF/n-BuOH=1/1	12M AcOH	120	No
38	DMF/n-BuOH=1/1	CF ₃ SO ₃ H	120	No
39	DMF/n-BuOH=1/1	TsOH	120	No
40	DMF/n-BuOH=1/1	2M TsOH	120	No
41	DMF/n-BuOH=1/1	4M TsOH	120	No
42	DMF/n-BuOH=1/1	6M TSOH	120	No

43	DMAC/n-BuOH =1/1	2M Na ₂ CO ₃	120	No
44	DMAC/n-BuOH =1/1	2M NaOH	120	No
45	DMAC/n-BuOH =1/1	2M KOH	120	No
46	DMAC/n-BuOH =1/1	Pyridine	120	No
47	DMAC/n-BuOH =1/1	Piperidine	120	No
48	DMAC/n-BuOH =1/1	Et ₃ N	120	No
49	DMAC/n-BuOH =1/1	AcOH	120	No
50	DMAC/n-BuOH =1/1	6M AcOH	120	No
51	DMAC/n-BuOH =1/1	12M AcOH	120	No
52	DMAC/n-BuOH =1/1	CF ₃ SO ₃ H	120	No
53	DMAC/n-BuOH =1/1	TsOH	120	No
54	DMAC/n-BuOH =1/1	2M TsOH	120	No
55	DMAC/n-BuOH =1/1	4M TsOH	120	No
56	DMAC/n-BuOH =1/1	6M TSOH	120	No
57	AcOH	4M TsOH	120	Low
58	AcOH/n-BuOH=1/1	4M TsOH	120	Low
59	AcOH/isopropanol=1/1	4M TsOH	120	Low
60	AcOH	4M TsOH	140	Moderate
61	AcOH/n-BuOH=1/1	4M TsOH	140	High
62	AcOH/isopropanol=1/1	4M TsOH	140	High

Table S3. Comparison of conductivity and carrier mobility between Janus dione based COFs and other conductive COFs.

COFs	Sample type	Methods	$\sigma/S \text{ cm}^{-1}$	Refs
NiPc-NH-CoPcF ₈	Film	4-probe	1.3×10^{-1}	S4
TFPPy-ICTO-COF	Pellet	4-probe	5.6×10^{-3}	S5
TFPPer-ICTO-COF	Pellet	4-probe	2.3×10^{-3}	S5
TBI-COF-O	Pellet	4-probe	7.5×10^{-4}	This work
Sp ² -c-COF	Pellet	2-probe	7.1×10^{-4} (dope)	S6
ZnPc-pz-I ₂	Pellet	Hall effect	3.1×10^{-4}	S7
CoPc-PDQ-COF	Pellet	4-probe	3.6×10^{-5}	S8
COF-DC-8	Pellet	4-probe	2.5×10^{-5}	S9
TBI-COF-N	Pellet	4-probe	2.3×10^{-5}	This work
TANG-COF	Pellet	4-probe	1×10^{-2} (dope)	S10
TFF-COF	Pellet	2-probe	2.1×10^{-7}	S11
TTF-Por(Co)-COF	Pellet	2-probe	1.3×10^{-7}	S12
TAPP-TFPP-COF	Pellet	2-probe	1.4×10^{-9}	S13

Table S4. Performance comparison between representative COF-based, metal oxides and organic small molecule materials for LIBs.

Electrode	Low-rate capacity	High-rate capacity	Ref
TBI-COF-O	320 mAh g ⁻¹ at 0.1C	245 mAh g ⁻¹ at 1C	This work
PT-COF50	267 mAh g ⁻¹ at 0.2 A g ⁻¹	229 mAh g ⁻¹ at 5 A g ⁻¹	S14
BTT-ICTO@CNT-50	396 mAh g ⁻¹ at 0.1 A g ⁻¹	227 mAh g ⁻¹ at 5 A g ⁻¹	S33
HATN-AQ-COF	319 mAh g ⁻¹ at 0.18 A g ⁻¹	227 mAh g ⁻¹ at 3.6A g ⁻¹	S15
TFPPy-ICTO-COF	338 mAh g ⁻¹ at 0.1 A g ⁻¹	214 mAh g ⁻¹ at 1 A g ⁻¹	S5
TBI-COF-N	265 mAh g ⁻¹ at 0.1C	204 mAh g ⁻¹ at 1C	This work
PIBN-G	271 mAh g ⁻¹ at 0.1C	193 mAh g ⁻¹ at 10C	S16
USTB-6@G	253 mAh g ⁻¹ at 0.1C	188 mAh g ⁻¹ at 10C	S34
PFG-1@rGO	480 mAh g ⁻¹ at 0.5 A g ⁻¹	189 mAh g ⁻¹ at 5 A g ⁻¹	S35
TFPPer-ICTO-COF	303 mAh g ⁻¹ at 0.1 A g ⁻¹	182 mAh g ⁻¹ at 1 A g ⁻¹	S5
PT-COF-30	280 mAh g ⁻¹ at 0.2 A g ⁻¹	145 mAh g ⁻¹ at 5 A g ⁻¹	S14
COF-TRO	268 mAh g ⁻¹ at 0.1C	124 mAh g ⁻¹ at 1C	S17
PT-COF10	225 mAh g ⁻¹ at 0.2 A g ⁻¹	115 mAh g ⁻¹ at 5 A g ⁻¹	S14
BTT-ICTO@CNT-30	326 mAh g ⁻¹ at 0.1 A g ⁻¹	113 mAh g ⁻¹ at 5 A g ⁻¹	S33
2D CCP-HATN	116 mAh g ⁻¹ at 0.1 A g ⁻¹	94 mAh g ⁻¹ at 0.1 A g ⁻¹	S18

PT-COF	193 mAh g ⁻¹ at 0.2 A g ⁻¹	76 mAh g ⁻¹ at 5 A g ⁻¹	S14
BTT-ICTO@CNT-10	269 mAh g ⁻¹ at 0.1 A g ⁻¹	67 mAh g ⁻¹ at 5 A g ⁻¹	S33
BTT-ICTO	225 mAh g ⁻¹ at 0.1 A g ⁻¹	65 mAh g ⁻¹ at 1 A g ⁻¹	S33
DAPH-TFPI-COF	80 mAh g ⁻¹ at 0.5C	50 mAh g ⁻¹ at 20C	S19
DAAQ-TFP-COF	110 mAh g ⁻¹ at 0.02 A g ⁻¹	25 mAh g ⁻¹ and at 3 A g ⁻¹	S20
2D-PAI@CNT	104.4 mAh g ⁻¹ at 0.1 A g ⁻¹	96 mAh g ⁻¹ at 2 A g ⁻¹	S21
PI-COF@rGO	112 mAh g ⁻¹ at 0.1C	67 mAh g ⁻¹ at 1C	S22
E-TP-COF	110 mAh g ⁻¹ at 0.2 A g ⁻¹	30 mAh g ⁻¹ at 2 A g ⁻¹	S23
NBALs	155 mAh g ⁻¹ at 0.5C	50 mAh g ⁻¹ at 20C	S24
C8Q	341 mAh g ⁻¹ at 0.2C	60 mAh g ⁻¹ at 5C	S25
PTN	119.1 mAh g ⁻¹ at 0.05 A g ⁻¹	89.4 mAh g ⁻¹ at 5 A g ⁻¹	S26
p-DNB	536 mAh g ⁻¹ at 0.05 A g ⁻¹	250 mAh g ⁻¹ at 0.2 A g ⁻¹	S27
1,5-DNN	Irreversible	Irreversible	S28
Li _{1.075} V _{0.925} O ₂	314 mAh g ⁻¹ at 0.1C	172 mAh g ⁻¹ at 5C	S29
Li _{0.78} V _{0.75} O ₂	551.6 mAh g ⁻¹ at 0.1 A g ⁻¹	272 mAh g ⁻¹ at 1 A g ⁻¹	S30
Li _{1.2} VO ₂	294 mAh g ⁻¹ at 0.1C	-	S31
Li _{1.07} V _{0.93} O ₂	116 mAh g ⁻¹ at 0.1C	-	S32

Section D. Supporting References.

- S1. E. Papajak, J. Zheng, X. Xu, H. R. Leverentz, D. G. Truhlar, *J. Chem. Theory Comput.*, 2011, **7**, 3027–3034.
- S2. S. Grimme, J. Antony, S. Ehrlich, H. Krieg, *J. Chem. Phys.*, 2010, **132**, 154104–154122.
- S3. S. S. Xantheas, *J. Chem. Phys.*, 1996, **104**, 8821–8824.
- S4. Y. Yue, P. Cai, X. Xu, H. Li, H. Chen, H. C. Zhou, N. Huang, *Angew. Chem. Int. Ed.*, 2021, **60**, 10806–10813.
- S5 X. Xu, S. Zhang, K. Xu, H. Chen, X. Fan, N. Huang, *J. Am. Chem. Soc.*, 2023, **145**, 1022–1030.
- S6. E. Jin, M. Asada, Q. Xu, S. Dalapati, M. A. Addicoat, M. A. Brady, H. Xu, T. Nakamura, T. Heine, Q. Chen, D. Jiang, *Science*, 2017, **357**, 673–676.
- S7. M. Wang, M. Wang, H. H. Lin, M. Ballabio, H. Zhong, M. Bonn, S. Zhou, T. Heine, E. Canovas, R. Dong, X. Feng, *J. Am. Chem. Soc.*, 2020, **142**, 21622–21627.
- S8. N. Huang, K. H. Lee, Y. Yue, X. Xu, S. Irle, Q. Jiang, D. Jiang, *Angew. Chem. Int. Ed.*, 2020, **59**, 16587–16593.
- S9. Z. Meng, R. M. Stolz, K. A. Mirica, *J. Am. Chem. Soc.*, 2019, **141**, 11929–11937.
- S10. V. Lakshmi, C. H. Liu, M. Rajeswara Rao, Y. Chen, Y. Fang, A. Dadvand, E. Hamzehpoor, Y. Sakai-Otsuka, R. S. Stein, D. F. Perepichka, *J. Am. Chem. Soc.*, 2020, **142**, 2155–2160.
- S11. S. L. Cai, Y. B. Zhang, A. B. Pun, B. He, J. Yang, F. M. Toma, I. D. Sharp, O. M. Yaghi, J. Fan, S. R. Zheng, W. G. Zhang, Y. Liu, *Chem. Sci.*, 2014, **5**, 4693–4700.
- S12. S. Jin, T. Sakurai, T. Kowalczyk, S. Dalapati, F. Xu, H. Wei, X. Chen, J. Gao, S. Seki, S. Irle, D. Jiang, *Chem. Eur. J.*, 2014, **20**, 14608–14613.
- S13. X. Xu, S. Wang, Y. Yue, N. Huang, *ACS Appl. Mater. Interfaces*, 2020, **12**, 37427–37434.
- S14. H. Gao, A. R. Neale, Q. Zhu, M. Bahri, X. Wang, H. Yang, Y. Xu, R. Clowes, N. D. Browning, M. A. Little, L. J. Hardwick, A. I. Cooper, *J. Am. Chem. Soc.*, 2022, **144**, 9434–9442.
- S15. X. Yang, L. Gong, X. Liu, P. Zhang, B. Li, D. Qi, K. Wang, F. He, J. Jiang, *Angew. Chem. Int. Ed.*, 2022, **61**, e202207043.
- S16. Z. Luo, L. Liu, J. Ning, K. Lei, Y. Lu, F. Li, J. Chen, *Angew. Chem. Int. Ed.*, 2018, **57**, 9443–9446.
- S17. X. Yang, Y. Hu, N. Dunlap, X. Wang, S. Huang, Z. Su, S. Sharma, Y. Jin, F. Huang, X. Wang, S. H. Lee, W. Zhang, *Angew. Chem. Int. Ed.*, 2020, **59**, 20385–20389.
- S18. S. Xu, G. Wang, B. P. Biswal, M. Addicoat, S. Paasch, W. Sheng, X. Zhuang, E. Brunner, T. Heine, R. Berger, X. Feng, *Angew. Chem. Int. Ed.*, 2019, **58**, 849–853.
- S19. E. Vitaku, C. N. Gannett, K. L. Carpenter, L. Shen, H. D. Abruna, W. R. Dichtel, *J. Am. Chem. Soc.*, 2020, **142**, 16–20.
- S20. S. Wang, Q. Wang, P. Shao, Y. Han, X. Gao, L. Ma, S. Yuan, X. Ma, J. Zhou, X. Feng, B. Wang, *J. Am. Chem. Soc.*, 2017, **139**, 4258–4261.
- S21. G. Wang, N. Chandrasekhar, B. P. Biswal, D. Becker, S. Paasch, E. Brunner, M. Addicoat, M. Yu, R. Berger, X. Feng, *Adv. Mater.*, 2019, **31**, 1901478.
- S22. Z. Wang, Y. Li, P. Liu, Q. Qi, F. Zhang, G. Lu, X. Zhao, X. Huang, *Nanoscale*, 2019, **11**, 5330–5335.
- S23. G. F. Zhao, H. N. Li, Z. H. Gao, L. F. Xu, Z. Y. Mei, S. Cai, T. T. Liu, X. F. Yang, H. Guo, X. L. Sun, *Adv. Funct. Mater.*, 2021, **31**, 2101019.
- S24 C. Luo, X. Ji, S. Hou, N. Eidson, X. Fan, Y. Liang, T. Deng, J. Jiang, C. Wang, *Adv. Mater.*, 2018, **30**, 1706498.
- S25. W. Huang, S. Liu, C. Li, Y. Lin, P. Hu, Z. Sun, Q. Zhang, *EcoMat*, 2022, **4**, e12214.

- S26. J. Wang, H. Liu, C. Du, X. Zhang, Y. Liu, H. Yao, Z. Sun, S. Guan, *Chem. Eng. J.*, 2022, **444**, 136598.
- S27. X. Liu, Z. Ye, *Adv. Energy Mater.*, 2021, **11**, 2003281.
- S28. Z. F. Chen, H. Su, P. F. Sun, P. X. Bai, J. X. Yang, M. J. Li, Y. F. Deng, Y. Liu, Y. H. Geng, Y. H. Xu, *Proc. Natl. Acad. Sci. U.S.A.*, 2022, **119**, e2116775119.
- S29. W. Kim, T. Y. U. Jeong, H. C. Choi, Y. J. Kim, J. H. Song, H. Lee, Y. J. J. Lee, *J. Appl. Electrochem.*, 2011, **41**, 803–808.
- S30. W. Q. Zhang, J. J. Luo, X. N. Li, J. W. Liang, Y. C. Zhu, Y. T. Qian, *J. Mater. Chem. A*, 2017, **5**, 5148–5155.
- S31. J. H. Song, H. J. Park, K. J. Kim, Y. N. Jo, J. S. Kim, Y. U. Jeong, Y. J. Kim, *J. Power Sources*, 2010, **195**, 6157–6161.
- S32. A. Armstrong, R. C. Lyness, P. M. Panchmatia, M. S. Islam, P. G. Bruce, *Nat. Mater.*, 2011, **10**, 223–229.
- S33. N. Fu, Y. Liu, K. Kang, X. Tang, S. Q. Zhang, Z. L. Yang, Y. Wang, P. J. Jin, Y. S. Niu, B. Yang, *Angew. Chem. Int. Ed.*, 2024, e202412334.
- S34. X. Liu, Y. Jin, H. Wang, X. Yang, P. Zhang, K. Wang, J. Jiang, *Adv. Mater.*, 2022, **34**, 2203605.
- S35. X. Li, H. Wang, H. Chen, Q. Zheng, Q. Zhang, H. Mao, Y. Liu, S. Cai, B. Sun, C. Dun, M. P. Gordon, H. Zheng, J. A. Reimer, J. J. Urban, J. Ciston, T. Tan, E. M. Chan, J. Zhang, Y. Liu, *Chem*, 2020, **6**, 933–944.